

On the influence of ice shelf edge position on circulation and water mass modification

Nadja Saleck¹, Hartmut H. Hellmer² and Eberhard Fahrbach²

¹Summer intern of Universität Oldenburg at²

²Alfred Wegener Institut für Polar and Meeresforschung
Columbusstrasse, D-27515 Bremerhaven, Germany

Introduction

The recent calving event in the southern Weddell Sea caused a significant southward retreat of the Ronne Ice Shelf edge (Oerter, this volume). Considered as a dynamical barrier for water mass exchange between the continental shelf and the ice shelf cavity (Grosfeld et al., 1997; Makinson and Nicholls, 1999) it was speculated during the FRISP Workshop held in Münster (July, 2000) whether this retreat might have an impact on shelf water circulation, cross-frontal exchange, and related ocean-ice shelf interaction.

Model Description

Focused on this question, we applied a terrain following (sigma coordinate) primitive equation model (SPEM; Haidvogel et al., 1991) to a rectangular box (640 km x 960 km) with 2/3 of the model domain occupied by the ice shelf cavity and 1/3 by the continental shelf in the “meridional” (y) direction. Model resolutions are 10 km in both horizontal directions and 12 layers in the vertical. For two simulations, bottom topography measured along two lines crossing the western and eastern Ronne Ice Shelf from the grounding line to the edge, c-c’ and d-d’, respectively, in Vaughan et al. (1994), were prescribed in the y-direction with no “zonal”(x) gradients (see schematics at the top of Figures 1 and 2). For an additional simulation, we introduced two depressions with different slopes along the western and eastern side of the model domain (Figure 3) approximating Ronne Basin and Filchner Trough (Schenke et al., 1998). Bottom depth always ranged from 1500 m at the southern boundary (grounding line) to 400 m at the northern boundary, the latter increasing to greater depth at the main axis of the troughs. The ice shelf thickness distribution only varied in the y-direction decreasing exponentially from 1300 m to 200 m (see figures showing meridional sections). The latter value increased/decreased as the position of the ice shelf edge moved southward/northward by 50 km (= 5 grid points). No surface forcing was applied on the continental shelf while in the cavity flux forcing resulted from the processes acting at the ocean/ice interface as described by Hellmer et al. [1998]. The model was initialized with constant fields for potential temperature, $\theta = -1.86$ °C, and salinity, $S = 34.5$. Model results are shown after 10 years of integration.

Results

The following Figures (1-3) are divided with regard to a northern (upper row), standard (central row), and southern (lower row) position of the ice shelf edge related to the transition from a flat to an inclined ocean floor.

The transport streamfunction distributions for the cavities without troughs (Figure 1) show that only for the southern position shelf water masses participate in the circulation with a significant cross-frontal exchange. In addition, for a constant bottom slope (Figure 1, right column) the intensity of the clockwise circulation in the cavity increases as the ice shelf edge retreats with only minor changes for the irregular slope. Here, the existence of three smaller circulation cells coinciding with the three steps in bottom topography (Figure 1, left column), the reduced inter-exchange, and the eastward intensification within the central cell document the strong impact of changes in water column thickness on the ambient vorticity field and related subice circulation.

For both cavity configurations, the basal mass flux (Figure 2a) shows the general pattern of enhanced melting in the deep southeastern corner of the model domain and freezing along the western boundary related to the ascending meltwater plume. With retreating ice shelf edge, the central region of low ice accumulation shrinks, and melting especially in a narrow band close to the edge increases due to warmer shelf water crossing and flowing parallel to the ice barrier. This general increase in melting is also documented by the annual mean freezing rates (upper left inserts) which almost double as the ice edge moves southward by 100 km. The greater increase as the edge moves from the standard to the southern position for the constant slope configuration compared to the case of irregular bottom slope is caused by the weakening of the northern subice cell. Representative for both configurations, the meridional section at $x = 50$ km for an irregular bottom slope (Figure 2b) shows a salinity increase of the ascending meltwater plume due to salt rejection during ice crystal formation along the western boundary. This plume has a slightly wider influence on shelf water salinities for a southerly edge position.

The major difference between the previous results and the results of the double-trough simulation (Figure 3) is the increase in cross-frontal exchange by almost an order of magnitude at the western side of the model domain. Although we used a scale different from Figure 1, the meridional shift of the ice edge influences more the transports on the continental shelf than into and within the ice shelf cavity (Figure 3a). The combination of topography and simple (= initialisation with constant temperature and salinity fields, no surface fluxes in the open ocean) thermohaline forcing produces cyclonic trough circulations which have been inferred from hydrographic measurements for the southern Weddell Sea continental shelf by Carmack and Foster (1977). A dominant subice circulation in the eastern trough does not exist allowing preconditioned water masses to participate in the western circulation.

Freezing rates also increased for the double-trough simulation (Figure 3b), but less than the transports, showing again a dependency on ice shelf edge position. The general horizontal pattern is the same with strong melting in the southeastern corner and high ice crystal accumulation along the western boundary of the model domain. The broad central regime of low accumulation (Figure 2a) reduced to a confined area above the western flank of the eastern trough comparable to the model results for the Filchner Ice Shelf (Grosfeld et al., 1998).

The salinity distribution along the western boundary ($x = 50$ km) shows that, compared to the non-trough simulation (Figure 2b), a strong trough circulation transports the meltwater plume northward at intermediate depth influencing the whole continental shelf water mass (Figure 3c). The obvious instability, saltier shelf water above fresher meltwater, for most of the continental shelf is temperature compensated due to the plume below the surface freezing point (not shown).

Conclusions

Our results show that the position of the ice shelf edge has an impact on the whole shelf circulation including the subice cavity. A southerly position increases the transports across the ice barrier influencing basal melting and the characteristics of the meltwater plume. However, it is not the position which controls the cross-frontal exchange but, as one might expect, the changes in water column thickness at the edge. Since the relative position of the ice barrier to the slope in bottom topography is important, only a detailed survey of the newly exposed sea floor could answer the question whether the retreat of the Ronne Ice Shelf edge increased the transport into the subice cavity and enhanced basal mass fluxes.

Although the percentage increase in basal melting as the ice edge moves south is higher for the simulations without zonal gradients in bottom topography, the double-trough model runs confirm that it is the exchange via the troughs which controls subice circulation and ocean/ice shelf interaction (Grosfeld et al., 1997). For the latter configuration, circulation and freezing patterns significantly differ from the observations and other model results. However, this would change for a more accurate cavity configuration with realistic temperature and salinity fields, prescribed or calculated for the continental shelf domain using a coupled sea-ice ocean model (e.g., Timmermann et al., 2000).

References

- Carmack, E. C., and T. D. Foster, Water masses and circulation in the Weddell Sea, in: *Polar Oceans, Proceedings of the Polar Oceans Conference, Montreal, May 1974*, edited by M.J. Dunbar, Arctic Institute of North America, pp. 151-165, 1977.
- Grosfeld, K., R. Gerdes, and J. Determann, Thermohaline circulation and interaction between ice shelf cavities and the adjacent open ocean, *J. Geophys. Res.*, 102(C7), 15,595-15,610, 1997.
- Grosfeld, K., H. H. Hellmer, M. Jonas, H. Sandhäger, M. Schulte, and D. G. Vaughan, Marine ice beneath Filchner Ice Shelf: Evidence from a multi-disciplinary approach, in: *Ocean, Ice, Atmosphere: Interactions at the Antarctic Continental Margin, Antarctic Res. Ser.*, 75, edited by S.S. Jacobs and R.F. Weiss, pp. 319-339, AGU, Washington, D.C., 1998.
- Haidvogel, D.B., J.L. Wilkin, and R.E. Young, A semi-spectral primitive equation ocean circulation model using vertical sigma and orthogonal curvilinear horizontal coordinates, *J. Comput. Phys.*, 94, 151-185, 1991.
- Hellmer, H.H., S.S. Jacobs, and A. Jenkins, Oceanic erosion of a floating Antarctic glacier in the Amundsen Sea, in: *Ocean, Ice, Atmosphere: Interactions at the Antarctic Continental Margin, Antarctic Res. Ser.*, 75, edited by S.S. Jacobs and R.F. Weiss, pp. 83-99, AGU, Washington, D.C., 1998.
- Makinson, K., and K. Nicholls, Modeling tidal currents beneath Filchner-Ronne Ice Shelf and the adjacent continental shelf: Their effect on mixing and transport, *J. Geophys. Res.*, 104(C6), 13,449-13,465, 1999.
- Schenke, H. W., H. Hinze, S. Dijkstra, B. Hoppmann, F. Niederjasper, and T. Schöne, The new bathymetric charts of the Weddell Sea: AWI BCWS, in: *Ocean, Ice, Atmosphere: Interactions at the Antarctic Continental Margin, Antarctic Res. Ser.*, 75, edited by S.S. Jacobs and R.F. Weiss, pp. 371-380, AGU, Washington, D.C., 1998.
- Timmermann, R., A. Beckmann, and H.H. Hellmer, Simulations of ice-ocean dynamics in the Weddell Sea. Part II: Interannual variability 1985-1993, submitted to *Journal of Geophysical Research*, 2000.
- Vaughan, D. G., J. Sievers, C. S. M. Doake, H. Hinze, D. R. Mantripp, V. S. Pozdeev, H. Sandhäger, H. W. Schenke, A. Solheim, and F. Thyssen, Subglacial and seabed topography, ice thickness and water column thickness in the vicinity of Filchner-Ronne Schelfeis, *Antarctica, Polarforschung*, 64(2), 75-88, 1994.

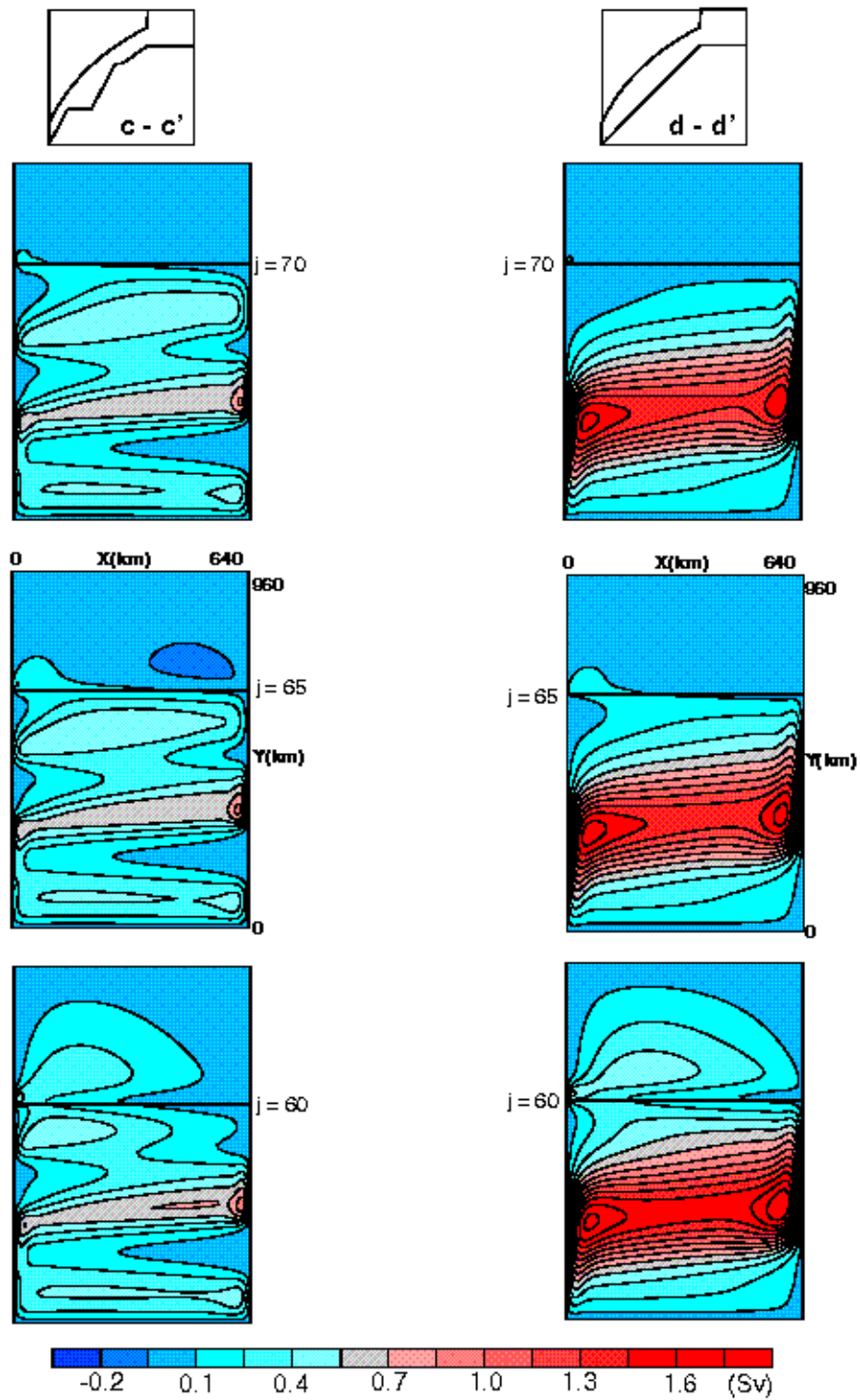


Figure 1: Transport streamfunctions for two different configurations approximating the western (irregular slope, left) and the eastern (constant slope, right) Ronne cavity (Vaughan et al., 1994). The position of the ice shelf edge varies meridionally with $j = 5$ (50 km). The central row shows the standard configurations plotted also as meridional sections at the top.

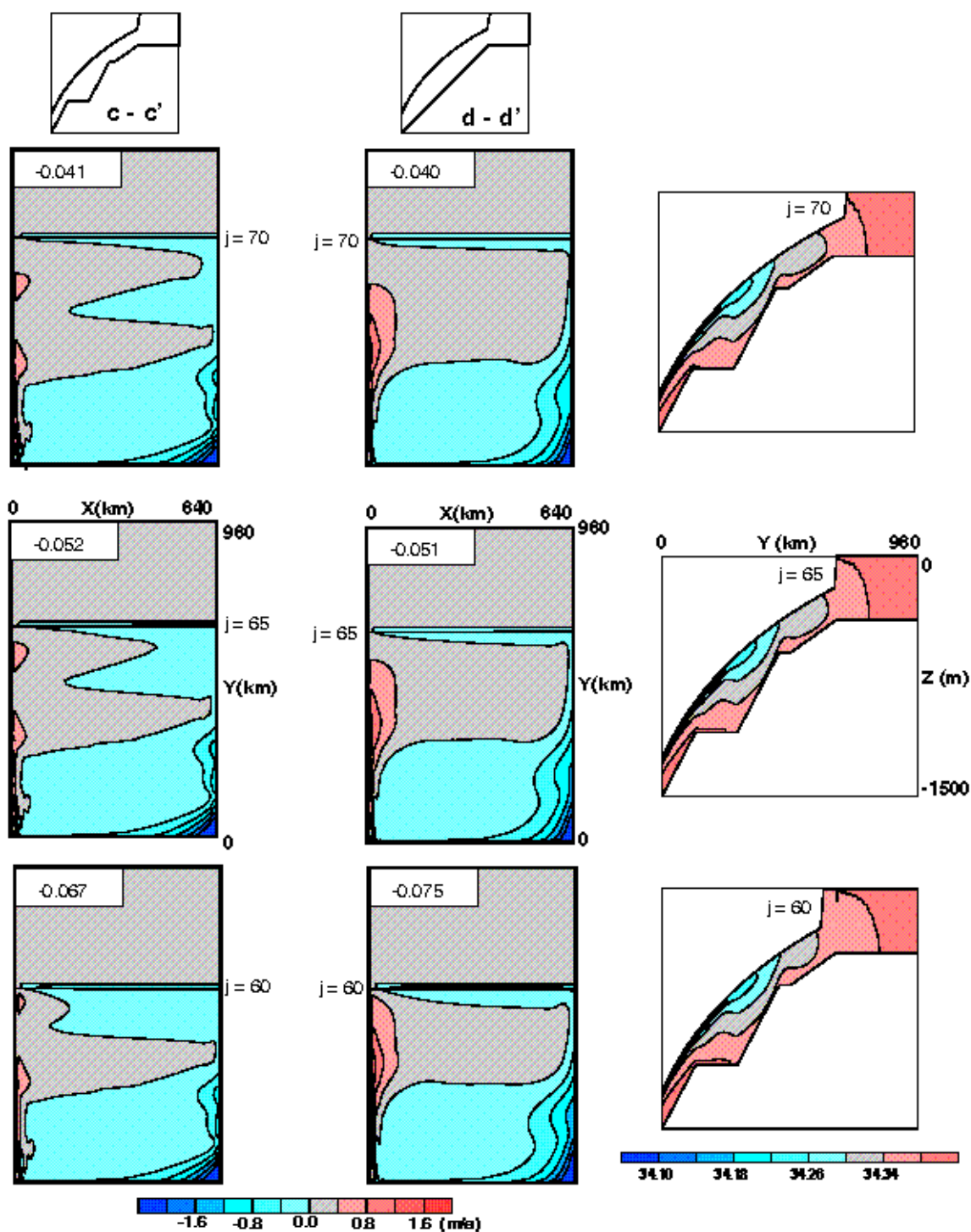


Figure 2a: Horizontal distribution of freezing rates (melting negative) for two different cavity configurations (same as Figure 1). The position of the ice shelf edge varies meridionally with $j = 5$ (50 km). The annual means for the whole cavity [m/a] are shown as inserts (upper left corner).

Figure 2b: Salinity distribution along the meridional section ($c - c'$) for $X = 50$ km. The ice shelf edge varies meridionally with $j = 5$ (50 km).

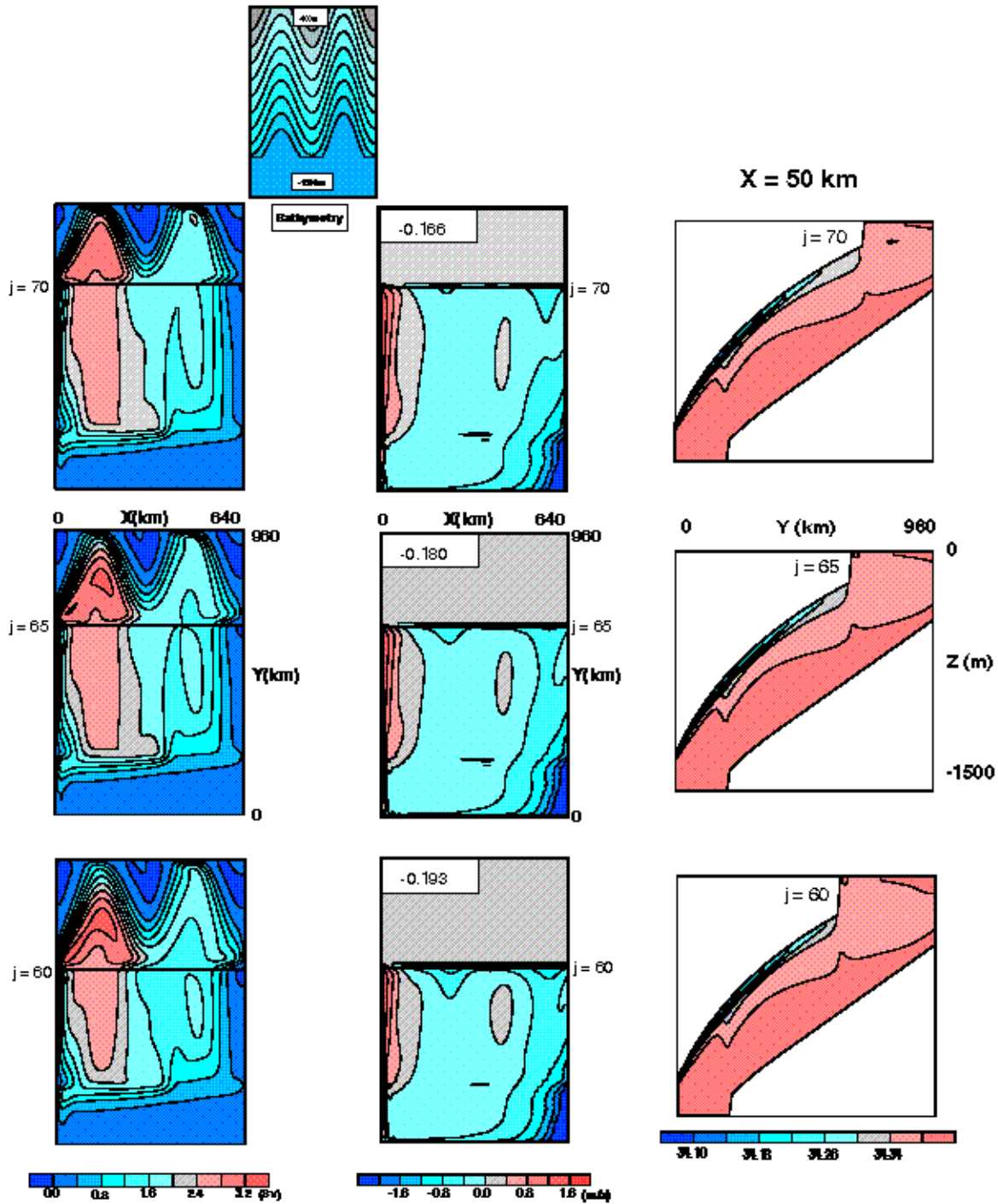


Figure 3a: Transport streamfunction for the double-trough topography (top panel). The position of the ice shelf edge varies meridionally with $j = 5$ (50 km).

Figure 3b: Horizontal distribution of freezing rates (melting negative). The annual means [m/a] for the whole cavity are shown in the inserts (upper left corner).

Figure 3c: Meridional salinity distribution at $X = 50$ km (freezing regime). The ice shelf edge varies meridionally with $j = 5$ (50 km).